Flow around an axially symmetrical slender body with perforated boundaries.

A. Skvortsov, M. Roberts, K. Gaylor, C. Norwood

Defence Science and Technology Organisation
506 Lorimer Street, Fishermans Bend, Vic 3207, Australia

Abstract

A simple model for the flow around a slender body with perforated boundaries is proposed. The model employs the framework of lubrication theory in which external flow is considered as a potential flow of incompressible fluid and flow inside the body can be well described by Poiseuille's solution. The Darcy boundary condition is imposed on the body surface. It is shown that the model can be reduced to one ODE which in some cases allows rather simple analytical treatment. Our analytical findings are supported by numerical simulations.

Introduction

Flow systems with permeable boundaries have been extensively studied in regard to the transport phenomena in geophysics, chemical engineering and biophysics (e.g. water and oil transport, mixing and filtration, microfluidics, cross-membrane traffic in cells, chemotaxis, etc) and there is a vast amount of literature accumulated on these topics (i.e. see [14], [2], [4], [8] and refs therein).

In application to the problems of aero– and hydro– dynamics the permeability (perforation) of the flow boundaries has been traditionally considered as one of the most effective means to control the flow structure in order to yield some favorable changes in the flow characteristics (delay of boundary layer turbulization, shift of flow separation point, decrease of aerodynamic noise, suppression of shock waves, etc). In particular, the most promising means of drag reduction are still based on additional fluxes across the perforated boundaries of the flow (i.e. sucking fluid from the boundary layer, injecting polymers or microbubbles) (see [3],[9],[13] and refs). All this necessitates the development of rather simple (i.e. analytically treatable), but still scientifically rigorous (e.g. based on clear physics principles) models for the flows with permeable boundaries, which can be used to promptly estimate the effect of boundary permeability on a particular flow system.

In this paper we present an analytical model of the incompressible flow around a slender body with perforated (i.e. permeable) boundaries. The model provides a simple analytical description of the phenomenon and rigorously defines controlling parameters of the flow. This is an extension of the model we developed for application to different flow systems [11], [10].

We hope that this model, once validated numerically and/or experimentally, can be used as as a tool for some optimisation studies and as a test case for more complex CFD models.

External Flow

Let us consider an axially symmetrical slender body in a uniform flow of incompressible inviscous fluid. The undisturbed flow velocity U coincides with the axis of the body (axis z). The shape (outer boundary) of the body is defined by the profile function $r_o(z)$. The ratio $\varepsilon = r_*/L$ ($r_* = \max(r_o)$, L is the body length) is considered to be a small parameter of the model, i.e. $\varepsilon \ll 1$.
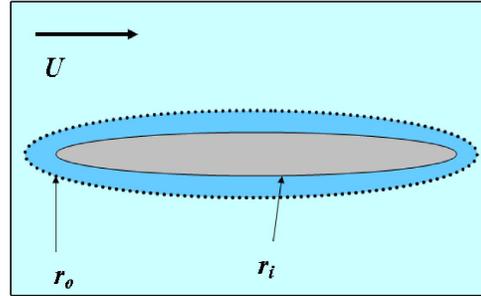

Figure 1: Geometry of the flow.

For the body with nonpermeable boundaries the pressure distribution p_o and the velocity potential ϕ are described by the well-known formulas from the slender body theory [15]

$$\frac{p_o}{\rho} = P_0 - U\phi' - \frac{\phi_r^2}{2}, \quad \phi = \frac{q}{2\pi}\ln r, \tag{1}$$

where $P_0 = U^2/2$, $q(z) = Us'$, $s(z) = \pi r_0^2$ is the cross-section of the body, $(\cdot)' \equiv d/dz$, $r^2 = x^2 + y^2$, $\phi_r = \partial\phi/\partial r$.

The second formula in (1) can eventually be generalised if we take into account the permeability of the boundary

$$q(z) = 2\pi r_0(r_0'U + V), \tag{2}$$

where $V(z)$ is the velocity associated with the cross-boundary flux.

The equation for V will be derived in the next section and we will employ an iterative approach. This implies that at the first step we set $V = 0$ (i.e. nonpermeable boundary) and use (1) for the external flow. Then with calculated V expression (2) provides a modified expression for the external flow with a finite permeability of the boundary being taken into account. For the second iteration we can use (2) and (1) for external pressure and to refine the equation for V and so on. In the context of the current paper we will consider only the first iteration.

In order for this iterative algorithm to converge, the following condition can be derived from (2)

$$r_0' \gg V/U. \tag{3}$$

We observe that it always holds for high velocity flow. We can also validate this condition retrospectively.

Model of Flow Inside the Body

To deduce the equation for V we employ some ideas of lubrication theory [1]. We assume that the interior of the body is formed by a space (cavity) between two shells (a perforated external shell $r_o(z)$ and a nonpermeable internal shell $r_i(z)$). Under a pressure difference, fluid can penetrate through the outer

shell and then flow in the cavity $r_o(z) \leq r \leq r_i(z)$. We consider a case when gap $h(z) = (r_o - r_i) \ll r_o(z)$ and the fluid flow in the cavity can be well described by Poiseuille's solution [15].

For the slender body geometry and for $h(z) \ll r_o(z)$ the direction of the flow in the cavity is very close to the direction of the z axis, so the direction perpendicular to the flow boundaries coincides with $\mathbf{r} = \{x, y\}$ (lateral radius-vector in cylindrical coordinate system). Following the well-known assumptions of the lubrication theory [1] we consider all derivatives in the z direction to be negligible in comparison with the derivatives in the $\mathbf{r}$ direction.

The flow across the outer surface of the body can be described by the Darcy-law expression

$$V = \widetilde{K}(p_i - p_o), \tag{4}$$

where V is the velocity of the flux across the boundary, $\widetilde{K} = K/d$, K is the hydraulic conductivity of the boundary, d is its thickness.[1]. Then we can easily write an equation for fluid discharge across the lateral cross-section of the cavity in terms of V:

$$\frac{dQ}{dz} = 2\pi r_o V, \tag{5}$$

where Q is the fluid discharge (a volume of fluid passing a cross-section of the cavity per unit of time). For Q we can use the classical formula for the Poiseuille's flow between coaxial cylinders [5]

$$Q = GB\frac{dp_i}{dz}, \tag{6}$$

where B is the "shape" function

$$B(z) \equiv B(r_o, r_i) = r_o^4 - r_i^4 - \frac{(r_o^2 - r_i^2)^2}{\ln(r_o/r_i)}, \tag{7}$$

$G = \pi/8\mu$, μ is the dynamic viscosity of the fluid. It is convenient to redefine the shape function in terms of the gap thickness $h(z) = (r_o(z) - r_i(z)) \ll r_o(z)$, so

$$B(z) \approx 4h^2 r_o^2. \tag{8}$$

From (4), (5), (6) it is apparent that our model can be reduced to one equation for p_i:

$$\frac{d}{dz}\left(B\frac{dp_i}{dz}\right) - \lambda r_o p_i = F, \tag{9}$$

where $\lambda = 2\pi\widetilde{K}/G = 16\mu K/d$ is the "permeability" scale,

$$F \equiv F(z) = -\lambda r_o p_o \tag{10}$$

and $p_o(z)$ is given by (1) evaluated at the body surface (i.e. with $r = r_o(z)$). By using (1) the expression for F can be rewritten in a form that explicitly depends on the body profile

$$F(z) = \frac{\rho U^2}{2}\lambda r_o\left[(r_o^2)'' \log(r_o) + \frac{1}{2}(r_o')^2\right]. \tag{11}$$

The boundary conditions for the solution of (9) can be derived from the symmetry arguments [11], [10]:

$$\frac{\partial p_i}{\partial z}(z=0) = \frac{\partial p_i}{\partial z}(z=L) = 0. \tag{12}$$

The equations (1), (2), (4), (9) provide a closed solution for the problem by enabling the calculations of flow inside and outside
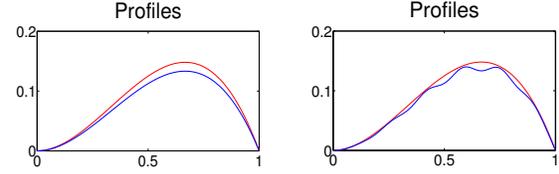

Figure 2: Body profiles used in numerical simulations: external r_o (red) and internal r_i (blue), see Eqs. (23) and (24).

of the body in term of profile functions $r_o(z), r_i(z)$, velocity of external flow U and permeability of the outer surface $\widetilde{K}$.

Preliminary Analysis

A comprehensive analytical treatment of the solutions of the model (1), (2), (9) is outside of the scope of this paper. Here we only briefly discuss some general properties of these solutions, which can provide insight into the flow structure, associated control options and can help to understand the results of numerical simulations.

As we can see from Eq. (9) the shape of body cavities (determined by profile $r_i(z)$) does not directly control the flow structure, but only through the shape function B (7), (8). Since B is the only parameter that consolidates the influence of the cavity shape it significantly simplifies our theoretical analysis by restricting it to the cases of limiting behavior of function $B(z)$. Recall, that in derivation of (9) we have not imposed any "smoothness" requirements on the profile $r_i(z)$, so for $r_i(z)$ (and hence for $B(z)$) we can assume rather intermittent distributions. Different distributions of $B(z)$ would correspond to the different perforation patterns and different cavity shapes (see Fig 2).

The first limiting case corresponds to the condition $B'(z)/L^3 \ll 1$ or $B(z) \approx B_0 = const$ (constant shape function). According to (8) it means that the cavity profile simply follows $h(z) \propto 1/r_o(z)$ for the majority of the length of the body and (9) can be reduced to

$$\overline{p}'' - \kappa\overline{p} = \overline{F}, \tag{13}$$

where $\overline{p} = 2p_i/\rho U^2$ is nondimensional pressure, $\overline{F} = 2F/\rho U^2$, $\kappa(z) = r_o(z)\lambda/B_0$. Then in nondimetional variables $\overline{z} = z/L \leq 1$, $r(z) = r_0/r_* = r_0/\varepsilon L$ this reads

$$p'' - \sigma^2 rp = \sigma^2 rf, \tag{14}$$

where

$$f = \left[(r^2)'' \log(r) + \frac{1}{2}(r')^2\right], \tag{15}$$

and

$$\sigma^2 = \varepsilon\lambda L^3/B_0 \approx \lambda L/4\varepsilon h_*^2, \tag{16}$$

with $h_* = \max(h(z))$. For the sake of notation simplicity we have dropped bars on nondimensional variables.

The parameter σ is the only nondimensional parameter of the problem that is responsible for a particular type of solution (i.e. flow structure). From this point of view it is the "aggregated" similarity parameter by changing which we can effectively control the global flow structure.

Since Eq. (14) is a linear ODE with variable coefficients its solution can be written in the standard form

$$p = p_1 + p_2, \tag{17}$$

[1]For a perforated boundary many analytical expression are available to represent K in terms of hole size, hole density and their distribution, see [14], [7] and refs therein

where p_1 is the homogeneous solution of (14) (i.e. with $f = 0$) and p_2 is any particular solution of the full equation (14). If the profile of the body is a slowly changing function (i.e. body shape is close to a straight circular cylinder) then $dr_o(z)/dz \ll 1$, hence f in (14) is small and $p_1 \gg p_2$.

The general properties of the solutions for p_1, p_2 can be easily established for the limit $\sigma \gg 1$ based on the WKB approximation. Following the text-book technique [6] we can write in this case

$$p_1 \approx \frac{c_1}{(r)^{1/4}} \exp\left[\frac{R(z)}{\sigma}\right] + \frac{c_2}{(r)^{1/4}} \exp\left[-\frac{R(z)}{\sigma}\right], \qquad (18)$$

where $R(z) = \int_0^z (r)^{1/2} dz$. For the p_2 we simply have

$$p_2 \approx f. \qquad (19)$$

From (18), (19) we can deduce an important property of the solution: it has a decent maximum/minimum wherever the function $R'(z) = 0$.

In general, the value of constants c_1, c_2 should be established from the boundary conditions (12) imposed on (17). Unfortunately, asymptotic solutions (18) diverge near $z = 0$ and $z = L$ (nose and tail of the body) and cannot be used for this purpose. This is a direct consequence of the well-known limitations of the WKB approximation [6]. To overcome this difficulty an improved approximation is required near $z = 0$ and $z = L$.

For the case $\sigma \ll 1$ it is straightforward to obtain an approximate solution of (14) in terms of the power-law series

$$r_0 \sim \sum_m a_m z^m, p_1 \sim \sum_m b_m z^m, \ \ p_2 \sim \sum_m d_m z^m, \qquad (20)$$

with a few first terms being already a good approximation. We will not discuss details of this procedure here.

In the opposite limit $B'(z)/L^3 \gg 1$ (rapidly changing shape function) we derive the following equation

$$B p'' + B' p' - \sigma^2 r p = \sigma^2 r f, \qquad (21)$$

where F is given by (15) and $B_0 = \max(B)$ in (16). The second term in LHS of this equation contains a derivative of the shape function and becomes dominant in the areas with the sharp changes of $B(z)$.

The behavior of the solutions of (21) can be understood based on the following qualitative arguments. Let us consider a piecewise distribution of $B(z)$. Within each domain with $B = const$ the solutions discussed above still hold. In order to include sharp changes (breaks) of B at the boundaries of the domains we need to impose appropriate boundary conditions on the solution for p. Since Eq.(9) is the second-order equation, we should impose two boundary conditions. The first condition is obvious, since $p(z)$ should be a continuous function (it is pressure), so we simply have to impose $p = const$. The second condition can be derived from Eq. (9) by integrating it across the domain boundary. Thus, we arrive at the second condition $p'B = const$. We can see that any break (or a sharp change) in the shape function $B(z)$ results in an associated change of the derivative p' while p remains continuous. In particular, we can expect that for any localised deformation of $B(z)$ (i.e. a "boss" mounted on some constant "background" B_0) the solution for $p(z)$ would be close to one with $B = B_0$, but with some deformation of the derivative p' corresponding to the position and the size of the "boss". From this it is also clear that even for an intermittent distribution of $B(z)$ (i.e. a random configuration of bosses) we can still

use (14) with the

$$B_0 \approx \frac{1}{L} \int_0^L B(z) dz \qquad (22)$$

as the first approximation for the solution of (21).

We found these arguments very useful for the "reverse-engineering" profile $r_i(z)$ (i.e. shape of the internal cavity), which can provide a desirable change in the external pressure distribution. This phenomenological approach provides a predictable means to locally control the flow system under consideration (global control is still best achieved by changing parameter σ defined by (16)). These qualitative conclusions are also supported by our numerical simulations (see below).

Expressions (17), (18), (19) provide illustrative examples of a variety of the solutions that can be produced by the proposed model (1), (2), (9).

Numerical Simulations

All simulations were performed in MATLAB where we employed a standard ODE solver. We calculated solutions of (1), (2), (4), (9) for the various body and cavity shapes. For illustration purposes we present here results for two set of profiles, corresponding to the smooth and the "wave-like" internal gap. The profile of the smooth gap was given by expressions

$$r_o/L = \varepsilon \bar{z}^2(\bar{z}-1), \ r_i = \gamma r_o, \qquad (23)$$

and the wave-like gap was modeled with

$$r_o/L = \varepsilon \bar{z}^2(\bar{z}-1), \ r_i = \gamma r_o(1+\zeta \sin^2(6\pi\bar{z})), \qquad (24)$$

where $\bar{z} = z/L$, $\gamma = 0.8$, $\varepsilon = 0.8$, $\zeta = 0.05$. The values of $\sigma = 0.0001$ and $\sigma = 0.00008$ were used for the first and second case.
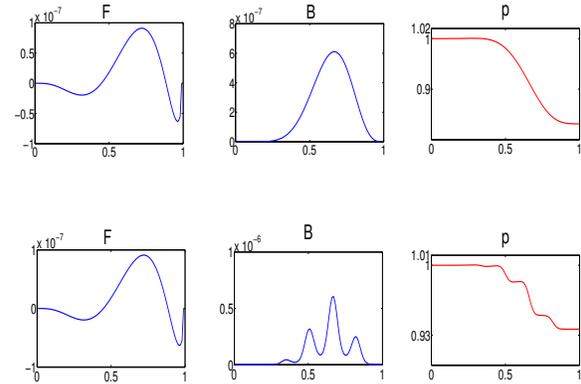

Figure 3: Examples of numerical solution of Eq (9). Columns: functions $F(z), B(z), p(z)$ (see text for details). Top row: solution for body profile (23), bottom row - for profile (24), see Fig 2. The horizontal axis of all graphs shows the relative distance from the leading edge of the body (ratio $\bar{z} = z/L$).

Profiles (23) and (24) are plotted in Fig.2. For a given set of profiles r_o, r_i we calculate functions $B(z)$ (7), $F(z)$ (11) and then solve Eq. (9) numerically. Results of our calculations are depicted in Fig 3.

Discussion and Future Work

We found that the results of our numerical simulations confirm properties of the analytical solutions described above. For instance, the plots presented at the top row in Fig.3 are from the family of solutions with slowly changing shape function

$B(z)$, while plots at the bottom row correspond with the rapid changes case. The deformations related to the maximums of function $B(z)$ ("bosses") discussed in the previous sections are also clearly visible. The comprehensive comparison of the analytical and numerical solutions of this model will be published elsewhere.

The proposed framework allows a number of generalisations to be made, that can be important for some practical applications. For instance, let us assume that cavity $r_i \leq r \leq r_o$ is filled with a porous material with permeability K_m. In such a case, equation (6) for discharge Q still holds, but now with

$$B(z) = 2\pi K_m(z)(r_o^2(z) - r_i^2(z)), \qquad (25)$$

where $K_m(z) = \mu \xi(z)$ is the distribution of the hydraulic conductivity of filling material along the cavity, $\xi(z)$ is its permeability.

In general, the flux across the boundary affects the external flow and the associated pressure distribution p_o. The equations describing this influence can be readily deduced from (1), (9), but in expression for p_o (10) we need to take into account the nonlinear terms associated with V in (2), (4) (so-called self-induced pressure gradient). Thus, we can arrive at

$$-p_o = \frac{\rho U^2}{2}\left[[r_o(r_o^{'} + v)]^{'}\log(r_o) + \frac{1}{2}(r_o^{'} + v)^2\right], \qquad (26)$$

where $v = \widetilde{K}(p_i - p_o)/U$.

From the mathematical point of view Eqs. (9), (26) form a nonlinear system of equations for two variables p_o, p_i that can be solved analytically or numerically. The nonlinear term $p_o p_i$ in this equation describes the influence of the internal flow (i.e. p_i) on the external pressure distribution (i.e. p_o) and manifests as a feedback in the flow system. The approximate solutions describing this feedback can be obtained iteratively (by assuming $\widetilde{K}$ as a small parameter) with the solutions presented above being the fist iteration. These solutions will be analysed in a sperate publication.

An important practical application of this theoretical research is a rigorous estimation of the effect of micro-perforation of the boundaries on the turbulent fluctuations in the boundary layer and associated flow noise [12]. Currently DSTO is developing a special test facility to enable investigation of such kind of effects in conjunction with other flow characteristics. The initial development plan for the facility (so-called buoyancy driven models) is to locate it in Lake St Clair in Tasmania. This lake provides a quiet, deep environment in which buoyancy driven models can be tested. DSTO has conducted a survey of the lake bottom and identified a number of areas with suitable bottom topography and depths varying from 60m to over 150m. The facility will incorporate a large "anchor" section which acts as the model docking and release station, and a series of hydrophone rings for flow noise measurement. Model instrumentation will include inertial accelerometers and a velocity probe so that the time to reach terminal velocity can be determined and the section of "constant speed" flight can be monitored. Noise measurements will be made using the ring hydrophones. The models will also be tested in the experimental hydrodynamic facilities at University of Tasmania in Launceston to measure drag coefficients. By varying the mass of the model, while maintaining the same external shape a series of terminal speeds can be measured; while interchangeable nose shapes and additional "add-on" sections for the model allow the perforation of the boundaries, the shape of the internal cavities and the overall drag coefficient to be varied.

The review of and attention to this kind of research was revived recently in light of the Collins class submarine replacement project.

Conclusions

We presented a theoretical model for the flow around a slender body with perforated boundaries, that allows analytical and numerical treatments for an arbitrary profiles of the body and for the internal cavity. We modelled the perforation of the outer surface of the body with the Darcy boundary conditions and assumed that the permeability of the surface is a small parameter. We derived expressions for the characteristics of the flow inside and outside the body and identified parameters that can be used for the effective flow control. Our results are supported by numerical simulations.

More extensive numerical validation will be required before we can proceed with the experimental validation of the model.

References

[1] Batchelor, G. K., An introduction to fluid mechanics, Cambridge Univ., 1976.

[2] Bird, R. B., Stewart, W. E. and Lightfoot. E. N., Transport phenomena, Second Edition, John Wiley & Sons, 2007.

[3] Bushnell, D. M., Aircraft drag reduction – a review. J. of Aerospace Eng., **217**, 1, 1-18, 2003.

[4] Cussler, E. L., Diffusion: mass transfer in fluid systems. Cambridge Univ, 1997

[5] Landau, L. D. and Lifshitz, E. M., Fluid mechanics, Elsevier Science, Second Edition, 2005.

[6] Landau, L. D. and Lifshitz, E. M., Quantum mechanics: Non-relativistic theory, Elsevier Science, Third Edition, 2003.

[7] Pozrikidis, C., Slip velocity over a perforated or patchy surface, J. Fluid Mech., **643**, 2010, 471–477.

[8] Procaccia, I. and L'vov, V. S., Theory of drag deduction by polymers in wall-bounded turbulence, Rev. of Mod. Physics, **80**, 225-247, 2008.

[9] Reneaux, J., Overview on drag reduction technologies for civil transport aircrafts, in: *Proc. Europ. Cong. Comp. Methods in App. Sciences and Eng.:ECCOMAS 2004*, 1-14, 2004.

[10] Roberts, M., Jamriska, M., Skvortsov, A. and McCallum, R., Study on aerosol penetration through clothing and individual protection equipment, DSTO Technical Report (AR-014-513), 2009.

[11] Roberts, M. and Skvortsov, A., A coupled air flow model for multi-layer protective clothing (submitted), 2010.

[12] Skvortsov, A., Gaylor, K., Norwood, C., Anderson, B., Chen, L., Scaling laws for noise generated by the turbulent flow around a slender body. in *Proc. Undersea Defence Technology:UDT Europe 2009*, 2009,182–186.

[13] Truong, V.T., Drag reduction technologies, DSTO Technical Report (AR-011-925), 2001.

[14] Truskey, G. A., Yuan, F. and Katz, D. F., Transport Phenomena in Biological Systems, Second Edition, Pearson Education, 2009.

[15] Whitham, G. B., Linear and nonlinear waves, John Wiley & Sons, 1999.